A late Holocene multi-proxy record from the northern Norwegian margin: temperature and salinity variability

Sarah MP Berben[1,*], Katrine Husum[2] and Steffen Aagaard-Sørensen[1]

[1]UiT - The Arctic University of Norway, Department of Geology, Tromsø, Norway

*Current affiliation: University of Bergen, Department of Earth Science and Bjerknes Centre for Climate Research, Bergen, Norway

[2]Norwegian Polar Institute, Fram Centre, Tromsø, Norway

Corresponding author: Sarah MP Berben (sarah.berben@uib.no)

Abstract

To elucidate the natural variability of Atlantic and Coastal water, a late Holocene multi-proxy analysis is performed on a marine sediment core from the northern Norwegian margin. This includes planktic foraminiferal fauna and their preservation indicators, stable isotopes ($\delta^{18}O_c$, $\delta^{13}C$), sub-surface temperature ($SST_{Mg/Ca}$) and salinity (SSS) records based on paired Mg/Ca and $\delta^{18}O_c$ measurements of *Neogloboquadrina pachyderma*, and transfer function derived sub-surface temperatures ($SST_{Transfer}$). The record shows a general cooling with subtle fluctuating palaeoceanographic conditions, here attributed to shifting North Atlantic Oscillation (NAO) modes. Period I (ca. 3500 – 2900 cal yr BP) is strongly influenced by Coastal water and stratified water masses, possibly correlating to negative NAO conditions. During period II (ca. 2900 – 1600 cal yr BP), dominating warm Atlantic water might be linked to a positive NAO mode and the Roman Warm Period. A renewed influence of Coastal water is observed throughout period III (ca. 1600 – 900 cal yr BP). Stable and colder SST values potentially correlate to the Dark Ages and are here attributed to negative NAO conditions. Within period IV (ca. 900 – 550 cal yr BP), the core site experienced a stronger influence of Atlantic water which might be due to positive NAO conditions correlating to the Medieval Warm Period. Additionally, an inverse correlation in Atlantic water influence between the eastern and western Atlantic Ocean is observed throughout period II, III and IV. This Atlantic oceanographic see-saw pattern is attributed to an opposite climatic response to changing NAO conditions arguing for a coupling between ocean and atmosphere.

Keywords

Atlantic water influence, Coastal water, NAO, northern Norwegian margin, late Holocene, multi-proxy record

Introduction

Throughout the late Holocene, a general cooling trend has been observed in the North Atlantic associated with a reduced influence of warm Atlantic water (e.g. Hald et al., 2007; Skirbekk et al., 2010; Slubowska et al., 2005). A similar cooling trend, recorded by lake and tree records from north-western Europe, has been ascribed to reduced insolation at high latitudes (e.g. Bjune et al., 2009; Kaufman et al., 2009). In contrast, fluctuations of a strengthened Atlantic water inflow towards the Arctic Ocean have been observed for the Vøring plateau (e.g. Andersson et al., 2003, 2010; Risebrobakken et al., 2003), the Barents Sea (e.g. Berben et al., 2014; Duplessy et al., 2001; Lubinski et al., 2001) and the Svalbard margin (e.g. Jernas et al., 2013; Slubowska-Woldengen et al., 2007; Werner et al., 2013; Zamelczyk et al., 2013). Furthermore, throughout the late Holocene, several observations of fluctuating climatic conditions have been found in the Nordic Seas (e.g. Giraudeau et al., 2004; Nyland et al., 2006; Slubowska-Woldengen et al., 2007; Solignac et al., 2006) as well as in north-western Europe (e.g. Bjune and Birks, 2008; Lauritzen and Lundberg, 1999). These include the "Roman Warm Period" (RWP; ca. BCE 50 – CE 400), the "Dark Ages" (DA; ca. CE 400 – 800), the "Medieval Warm Period" (MWP; CE 900 – 1500) and the "Little Ice Age" (LIA; ca. CE 1500 – 1900) (e.g. Lamb, 1977). As Atlantic water inflow towards the Arctic Ocean is part of the Atlantic Meridional Overturning Circulation (AMOC) it is not only contributing to

53 climatic conditions in north-western Europe, but also affecting the global climate
54 system (e.g. Vellinga and Wood, 2002).

55 These fluctuating conditions have been ascribed to different causes such as solar
56 forcing, volcanic eruptions (e.g. Bryson and Goodman, 1980; Jiang et al., 2005; Lean,
57 2002; Wanner et al., 2008) or changes in atmospheric forcing linked to the North
58 Atlantic Oscillation (NAO) which influence the inflow of Atlantic water to the Arctic
59 Ocean (e.g. Olsen et al., 2012; Trouet et al., 2009). Additionally, NAO fluctuations have
60 also been suggested to result in opposite climatic trends between the subpolar North
61 Atlantic and the Norwegian Sea during the late Holocene (Miettinen et al., 2011, 2012).

62 Warm and salty Atlantic water is brought into the Nordic Seas by the North
63 Atlantic Current (NAC) which flows parallel with colder and less saline Coastal water
64 along the Norwegian margin. These two water masses possess opposite characteristics
65 with respect to temperature and salinity. Further, they respond opposite to the
66 strengthened or reduced westerlies attributed to positive or negative NAO modes (e.g.
67 Sætre, 2007). A positive versus negative NAO mode affects the climatic conditions in
68 north-western Europe by generating warmer and wetter versus colder and dryer
69 conditions (e.g. Wanner et al., 2001). Along the Norwegian coast the impact of the
70 variable NAO is seen in precipitation, temperature and wind intensity changes (Ottersen
71 et al., 2001). Thus, the northern Norwegian margin is a key location to investigate the

natural variability of Atlantic water inflow throughout the late Holocene linked to fluctuating NAO modes.

For the Nordic Seas, several studies have reconstructed water mass properties based on planktic foraminiferal fauna. Transfer functions reflect sub-surface temperatures whereas stable oxygen isotopes reflect both the temperature and the stable oxygen isotopic composition of ambient sea water ($\delta^{18}O_w$) (e.g. Berben et al., 2014; Rasmussen and Thomsen, 2010; Risebrobakken et al., 2003). In addition, paired calcite $\delta^{18}O_c$ and Mg/Ca measurements enable the reconstruction of a palaeo sub-surface temperature and salinity record (e.g. Elderfield and Ganssen, 2000; Elderfield et al., 2010; Kozdon et al., 2009; Mashiotta et al., 1999; Thornalley et al., 2009).

In this study, the distribution of planktic foraminiferal fauna in a marine sediment core from the northern Norwegian margin is presented. Additionally, the preservation conditions as well as paired Mg/Ca and stable isotope ($\delta^{18}O_c$, $\delta^{13}C$) measurements of *Neogloboquadrina pachyderma* have been analysed by Berben (2014). This multi-proxy dataset represents the variability of both palaeo sub-surface temperature and salinity values. Hence, it is analysed in order to investigate the fluctuating interplay of Atlantic and Coastal water related to variable NAO modes throughout the late Holocene.

Present day oceanography

92 The Norwegian Sea is dominated by relatively warm and saline Atlantic water (>2 °C,
93 >35 ‰; Hopkins, 1991). Atlantic water is brought to the area by the two-branched
94 Norwegian Atlantic Current (NwAC) (Orvik and Niiler, 2002) (Figure 1a). Both
95 branches follow a topographically steered northwards pathway through the Nordic Seas
96 and eventually reach the Arctic Ocean via the Fram Strait. The eastern branch passes
97 through the Faroe-Shetland channel and continues a pathway along the Norwegian shelf
98 edge towards the Arctic Ocean with a branch flowing into the Barents Sea (Orvik and
99 Niiler, 2002) (Figure 1a). The western branch crosses the Iceland-Faroe Ridge entering
100 the Norwegian Sea as the Iceland-Faroe frontal jet (Perkins et al., 1998) (Figure 1a).
101 Variability in the lateral (east-west) extent of the NwAC is mainly controlled by the
102 intensity of the westerly winds associated with the NAO. In particular, an
103 increased/decreased NAO index leads to a narrower/broader current (Blindheim et al.,
104 2000). In addition, south of Iceland, Atlantic water is transported south-westwards by
105 the Irminger Current (IC) where it is then incorporated into the West Greenland Current
106 (WGC) (Hopkins, 1991; Hurdle, 1986) (Figure 1a) [insert Figure 1].
107 The Norwegian Coastal Current (NCC) transports Coastal water (2-13 °C, 32-35
108 ‰; Hopkins, 1991) northwards originating from the North Sea, the Baltic and the
109 Norwegian coast (Figure 1a). Coastal water is characterized by its low salinities due to
110 the influence of freshwater run off from the Norwegian mainland. The NCC is density
111 driven which is mainly influenced by its salinity distribution (Sætre, 2007). Mixing with

Atlantic water increases northwards and thus, salinity increases whereas stratification reduces. In general, cold Coastal water can be found above warmer Atlantic water in the upper 50 to 100 m of the water column as a thinning wedge westwards (Ikeda et al., 1989) (Figure 1b). A boundary is formed as a well-defined oceanic front between the cold, low salinity Coastal water and the warmer, more saline Atlantic water (Ikeda et al., 1989). The overall properties and movements of the NCC are influenced by several factors such as freshwater, tides, wind conditions, bottom topography and Atlantic water (Sætre, 2007). In the study area, the topography causes the NCC to extend much further westwards and hence, closer to the influence of the NwAC (Figure 1c).

Material and methods

For this study, a marine sediment core from the northern Norwegian margin (Vøring plateau in front of Trænadjupet south of the Lofoten) was investigated. The core (W00-SC3) (67.24° N, 08.31° E) was retrieved in 2000 by the SV *Geobay* at a water depth of 1184 m (Laberg et al., 2002) (Figure 1). Its recovery was 385 cm from which the top 19 cm was disturbed and therefore not used. The core consists of very soft clay sediments (Laberg et al., 2002) and was sampled for every cm between 19 and 263 cm.

Chronology

A depth-age model of W00-SC3 based on four AMS ^{14}C dates measured on *N. pachyderma* was developed (Table 1). All four AMS ^{14}C dates were calibrated using Calib 7.0.0 software (Stuiver and Reimer, 1993), the Marine13 calibration curve (Reimer et al., 2013) and a local reservoir age (ΔR value) of 71 ± 21 following Mangerud et al. (2006). The calibration was constrained on a 2-σ range for both calendar years Before Present (cal yr BP) and calendar years Before Common Era (BCE)/Common Era (CE) (cal yr BCE/CE). For this study, the cal yr BP depth-age model will be used, however, the cal yr BCE/CE scale was added for all plotted data in order to compare with different studies. The AMS ^{14}C date at 23.5 cm was omitted from the final depth-age model as it appeared too old. The new depth-age model was constrained using a linear interpolation between the dated levels. Further, based on the homogeneous lithology throughout the core, the sedimentation rate from 120 - 40 cm was extrapolated towards the top, more specifically between 40 and 19 cm (Figure 2). The resulting depth-age model is constrained between 3485 and 550 cal yr BP (1536 BCE – 1395 CE) and shows sedimentation rates between 0.79 and 0.87 mm/year enabling a multi-decadal temporal resolution (Figure 2). Nonetheless, due to the low number of AMS ^{14}C dates of this age model, the final interpretation is focused on a centennial temporal resolution [insert Figure 2].

150 **Table 1.** AMS ^{14}C dates and calibrated radiocarbon ages of W00-SC3. The calibration is performed using
151 Calib 7.0.0 software (Stuiver and Reimer, 1993), the Marine13 calibration curve (Reimer et al., 2013) and
152 a local reservoir age (ΔR value) of 71 ± 21 following Mangerud et al. (2006). The AMS ^{14}C date
153 highlighted in grey is omitted from the final depth-age model.

Lab ID	Core depth (cm)	Material	Uncorrected ^{14}C age	cal yr BP	2-σ range BP	cal yr BCE/CE	2-σ range BCE/CE	Reference
Beta-334422	23.5	*N. pachyderma*	1590 ± 30	1069	968 - 1170	881 CE	780 - 982 CE	This study
TUa-2931	40.0	*N. pachyderma*	1360 ± 65	821.5	684 - 959	1128.5 CE	991 - 1266 CE	Laberg et al., 2002
TUa-2930	120.0	*N. pachyderma*	2305 ± 55	1836	1688 - 1984	114.5 CE	35 BCE - 262 CE	Laberg et al., 2002
TUa-2929	263.0	*N. pachyderma*	3660 ± 95	3484.5	3237 - 3732	1535.5 BCE	1783 - 1288 BCE	Laberg et al., 2002

154

155 *Sub-surface water mass properties*

156 All samples were freeze-dried, wet-sieved through three different size fractions (1000,
157 100 and 63 μm) and subsequently dried at 40 °C. Sixty-two samples from every 4 cm
158 from the 100 - 1000 μm size fraction were analysed for their planktic foraminiferal
159 content (>300 specimens) following Knudsen (1998). The identification of left and right
160 coiling *N. pachyderma* was done following Darling et al. (2006), meaning that the right
161 coiling form is identified as *Neogloboquadrina incompta* (Cifelli, 1961). Subsequently,
162 relative abundances (%) of each species, planktic foraminiferal concentration (#/g
163 sediment), and fluxes (#/cm^2/yr) were calculated. For the latter, a theoretical value for
164 the dry bulk density of 0.76 g/cm^3 was assumed based on marine sediment core T-88-2

retrieved nearby the study site (Aspeli, 1994) and subsequently, calculated according Ehrmann and Thiede (1985).

Carbonate dissolution might affect the planktic foraminiferal assemblages, hence it is necessary to investigate the preservation conditions in order to assess the potential dissolution induced pre- and post-depositional alterations (e.g. Zamelczyk et al., 2013). Preservation indicators such as the mean shell weight (µg) of *N. pachyderma* (118 samples) (Barker and Elderfield, 2002; Beer et al., 2010; Broecker and Clark, 2001) and fragmentation (%) of planktic foraminiferal tests (62 samples) (Conan et al., 2002) were investigated. The latter was calculated using the equation of Pufhl and Shackleton (2004). For the mean shell weight, a strict selection of four-chambered, square-shaped and visually well preserved forms from the same morphotype, combined with an optimum sample size of 50 specimens were selected from a narrow size range (150 - 250 µm) in order to minimize problems of size and/or ontogeny variations (Broecker and Clark, 2001; Barker et al., 2004). Additionally, the weight percentages (wt. %) of total carbon (TC) and total organic carbon (TOC) were analysed for 244 samples. Subsequently, the calcium carbonate content ($CaCO_3$) in weight percentages (wt. %) was calculated following Espitalié et al. (1977).

Sub-surface water mass properties such as temperature and salinity, as well as primary production and stratification characteristics, are reflected by the stable oxygen and carbon isotopic compositions of foraminiferal calcite (e.g. Katz et al., 2010;

185 Spielhagen and Erlenkeuser, 1994). From the W00-SC3 sediment core, 117 stable
186 isotope ($\delta^{18}O_c$, $\delta^{13}C$) measurements (‰ vs. VPDB) were carried out using *N.*
187 *pachyderma* from the 150 - 250 µm size fraction. The measurements were performed
188 with a Finnigan MAT 253 mass spectrometer coupled to an automated Kiel device at
189 the Geological Mass Spectrometer (GMS) Laboratory of the University of Bergen.
190 Analytical errors are respectively ±0.06 ‰ and ±0.03 ‰ for $\delta^{18}O_c$ and $\delta^{13}C$
191 measurements. Further, a vital effect of 0.6 ‰ was applied on the $\delta^{18}O_c$ measurements
192 following previous studies from the area (Nyland et al., 2006; Simstich et al., 2003).
193 Quantitative reconstructions of summer sub-surface temperatures (°C) at 100 m
194 water depth ($SST_{Transfer}$) was done using a WA-PLS transfer function and a modern
195 analogue dataset based on the >100 µm size fraction (Husum and Hald, 2012). Further,
196 reconstructions of both sub-surface temperature ($SST_{Mg/Ca}$) and salinity (SSS) were
197 based on a combined analysis of the Mg/Ca ratio (mmol/mol) and stable oxygen
198 isotopic composition ($\delta^{18}O_c$) of *N. pachyderma* (Berben, 2014). In order to calculate the
199 $SST_{Mg/Ca}$ record (°C), the species-specific temperature:Mg/Ca equation of Kozdon et al.
200 (2009) was used, whereas to calculate SSS values (‰), the salinity to $\delta^{18}O_w$ relation by
201 Simstich et al. (2003) was applied.
202

203 ## Results

204 *Planktic foraminifera*

205 The planktic foraminiferal fauna consist of six species: *N. pachyderma*, *Turborotalita*
206 *quinqueloba*, *N. incompta*, *Globigerinita glutinata*, *Globigerina bulloides* and
207 *Globigerinita uvula* (Table 2) (Figure 3). Overall, the record is dominated by *N.*
208 *incompta* and *T. quinqueloba* with a mean value of ca. 34 and 29 % (Figure 3c and 3d)
209 [insert Figure 3].
210
211 **Table 2.** Planktic foraminiferal species list.

Planktic foraminiferal species
Globigerina bulloides (d'Orbigny), 1826
Globigerinita glutinata (Egger), 1893
Globigerinita uvula (Ehrenberg), 1861
Neogloboquadrina incompta (Cifelli), 1961
Neogloboquadrina pachyderma (sinistral) (Ehrenberg), 1861
Turborotalita quinqueloba (Natland), 1838

212
213 Between ca. 3500 and 2900 cal yr BP, the planktic foraminiferal concentration
214 and flux show relative low values of ca. 563 #/g sediment and ca. 41 #/cm^2/yr (Figure
215 3a and 4e). *N. pachyderma* and *N. incompta* show a decrease from ca. 18 to 12 % and
216 from ca. 40 to 19 % (Figure 3b and 3c). Simultaneously, *T. quinqueloba* and *G. uvula*
217 increase from ca. 28 to 36 % and from ca. 5 to 21 % (Figure 3d and 3g).
218 Both the planktic foraminiferal concentration and flux show slightly higher
219 values of ca. 948 #/g sediment and ca. 63 #/cm^2/yr between ca. 2900 and 2300 cal yr
220 BP, and are followed by a sharp increase (Figure 3a and 4e). The highest recorded

values in this study (3765 #/g sediment and 226 #/cm^2/yr) are reached just before ca. 1600 cal yr BP (Figure 3a and 4e). At ca. 1600 cal yr BP, a profound decrease in planktic foraminiferal concentration and flux is noticed, showing a drastic change from high to relatively low values (from 3765 to 865 #/g sediment and from 226 to 52 #/cm^2/yr, respectively). Further, between ca. 2900 and 1600 cal yr BP, the abundances of *N. pachyderma* are relatively stable around 12 %, *N. incompta* shows high and stable values of ca. 33 % and *T. quinqueloba* shows also high values (ca. 31 %) albeit with a moderate decrease towards ca. 1600 cal yr BP (Figure 3b, 3c and 3d). *G. glutinata* and *G. bulloides* show, in particular between ca. 2900 and 2300 cal yr BP, the highest recorded values of this study (5 and 4 %) followed by slightly reduced values towards ca. 1600 cal yr BP (Figure 3e and 3f).

At ca. 1600 cal yr BP, the strong shift from high to low planktic foraminiferal concentration and flux is followed by stable values between ca. 1600 and 900 cal yr BP (ca. 1330 #/g sediment and ca. 80 #/cm^2/yr) (Figure 3a and 4e). In addition, the relative abundances of *G. glutinata* and *G. uvula* increase from ca. 2 to 4 % and from ca. 15 to 27 % (Figure 3e and 3g). Further throughout this time interval, *T. quinqueloba* shows a slight decrease from ca. 25 to 20 % (Figure 3d), whereas the abundances of the remaining species stay relatively constant (Figure 3b, 3c and 3f).

Between ca. 900 and 550 cal yr BP, the concentration and flux records slightly decrease towards 450 #/g sediment and 27 #/cm^2/yr (Figure 3a and 4e). Most

241 interesting in the faunal record is the clear decreasing shift in *G. uvula* starting at ca.
242 900 cal yr BP (Figure 3g). Its relative abundance decreases from ca. 27 % towards ca. 8
243 % between ca. 900 and 550 cal yr BP (Figure 3g). Simultaneously, *N. pachyderma* and
244 *N. incompta* show the opposite shift towards values up to ca. 23 and 42 %, respectively,
245 at the top of the record (Figure 3b and 3c).
246
247 *Preservation indicators*

248 Between ca. 3500 and 2900 cal yr BP, the planktic foraminiferal fragmentation shows
249 generally high values around ca. 74 %, whereas the mean shell weight of *N.*
250 *pachyderma* varies around ca. 3.3 µg (Figure 4a and 4b). The fragmentation remains
251 relatively stable around slightly reduced values (ca. 68 %) between ca. 2900 and 1600
252 cal yr BP (Figure 4a). At ca. 2900 cal yr BP, the mean shell weight decreases towards
253 1.7 µg at ca. 2300 cal yr BP where after an increase reaching ca. 3 µg is followed at ca.
254 1600 cal yr BP (Figure 4b). Between ca. 1600 and 900 cal yr BP, the mean shell weight
255 remains stable around slightly reduced values of ca. 2.6 µg. Both preservation indicators
256 show a pronounced increase from ca. 75 to 90 % and from 2.4 to 3.2 µg between ca.
257 900 and 550 cal yr BP (Figure 4a and 4b) [insert Figure 4].
258
259 *Geochemical analysis*

Both TOC and $CaCO_3$ records show, between ca. 3500 and 2900 cal yr BP, an increase of ca. 0.7 to 1.0 wt. % for TOC and ca. 17 to 22 wt. % for $CaCO_3$ (Figure 4c and 4d). Towards ca. 2300 cal yr BP, increasing TOC values reach 1.1 wt. % where after a sudden drop to 0.8 wt. % is followed around ca. 2200 cal yr BP (Figure 4c). Further, this record remains stable around this value towards ca. 1600 cal yr BP. Between ca. 2900 and 1600 cal yr BP, the $CaCO_3$ record continues its increasing trend from ca. 22 to 30 wt. % and starts to decrease at ca. 1600 cal yr BP (Figure 4d). This decline reaches a value of ca. 26 wt. % at ca. 900 cal yr BP. Additionally, TOC values gradually increase between ca. 1600 and 900 cal yr BP from 0.9 to 1.0 wt. %. Further, TOC values remain relatively stable around ca. 1.0 wt. %, whereas the $CaCO_3$ record increases slightly towards ca. 26 wt. % between ca. 900 and 550 cal yr BP (Figure 4c and 4d).

Stable isotope analysis

Between ca. 3500 and 2900 cal yr BP, the $\delta^{13}C$ record shows increasing values from ca. 0.2 to 0.4 ‰, whereas $\delta^{18}O_c$ values decrease moderately from ca. 2.9 to 2.8 ‰ (Figure 5a and 5b). At ca. 2900 cal yr BP, the $\delta^{13}C$ values decrease from ca. 0.4 ‰ towards ca. 0.1 ‰ at ca. 2300 cal yr BP (Figure 5a). Thereafter, they are followed by relatively stable values (ca. 0.3 ‰) towards ca. 1600 cal yr BP. Simultaneously, the $\delta^{18}O_c$ record continues its decreasing trend reaching 2.5 ‰ at ca. 1600 cal yr BP (Figure 5b). After ca. 1600 cal yr BP, the $\delta^{13}C$ values increase again, in particular from 0.2 ‰ up to 0.4 ‰

280 at ca. 900 cal yr BP (Figure 5a). Throughout the latter time interval, the $\delta^{18}O_c$ values
281 initially continue their decreasing trend reaching 2.4 ‰ at ca. 1300 cal yr BP before an
282 increase up to ca. 2.7 ‰ is recorded between ca. 1200 and 900 cal yr BP (Figure 5b).
283 At ca. 900 cal yr BP, both records increase simultaneously towards ca. 550 cal yr BP
284 reaching values of ca. 0.5 ‰ for $\delta^{13}C$ and ca. 2.8 ‰ for $\delta^{18}O_c$ (Figure 5a and 5b) [insert
285 Figure 5].
286
287 *Sub-surface temperature and salinity reconstructions*

288 The $SST_{Transfer}$ record shows a decrease from 7.2 to 6.8 °C between ca. 3500 and 2900
289 cal yr BP (Figure 3h and 6c). At ca. 2900 cal yr BP, a sharp increase in $SST_{Transfer}$ is
290 followed by relatively high values around (ca. 7.4 °C) till ca. 2300 cal yr BP.
291 Thereafter, the $SST_{Transfer}$ record decreases reaching a value of ca. 6.8 °C at ca. 1600 cal
292 yr BP. Here after, the $SST_{Transfer}$ record stops its decreasing trend and stabilizes around
293 the value of ca. 6.6 °C until ca. 900 cal yr BP. Eventually, after ca. 900 cal yr BP, the
294 $SST_{Transfer}$ record shows a slight decrease towards ca. 6.3 °C at the top of the record
295 [insert Figure 6].

296 Between ca. 3500 and 3300 cal yr BP, the $SST_{Mg/Ca}$ values show a small
297 decrease from 3.1 to 2.7 °C followed by relatively stable values of ca. 3.3 °C until ca.
298 2900 cal yr BP (Figure 6b). Further, between ca. 2900 and 2500 cal yr BP, the $SST_{Mg/Ca}$
299 values show a gradual increase from ca. 3.0 to 4.2 °C which are followed by relative

300 stable values (ca. 3.5 °C) between ca. 2100 and 1600 cal yr BP. Then, around ca. 1600
301 cal yr BP, the $SST_{Mg/Ca}$ record shows an initial decrease towards 2.7 °C at ca. 1500 cal
302 yr BP, where after lower values of ca. 3.2 °C are recorded, albeit with one exception of
303 a single peak (4.7 °C) around ca. 1300 cal yr BP.

304 Between ca. 3500 and 2900 cal yr BP, the reconstructed SSS record shows a
305 gradual decrease from ca. 34 to 32 ‰ (Figure 6d). After ca. 2900 cal yr BP, the SSS
306 values increase to 34 ‰ at ca. 2800 cal yr BP followed by a decrease until ca. 2500 cal
307 yr BP. Between ca. 2100 and 1600 cal yr BP, the palaeo SSS record is stable around ca.
308 33 ‰, showing the highest values of the record (i.e. 34.0 ‰). At ca. 1600 cal yr BP, the
309 SSS record drops, where after it continues with lower and stable values (ca. 32 ‰) till
310 ca. 900 cal yr BP.

311

312 ## Palaeoceanographic evolution of the late Holocene

313 Throughout the late Holocene, the current proxy records show an overall cooling, e.g.
314 the $SST_{Transfer}$ values decrease from 7.7 to 6.3 °C (Figure 3h and 6c). This general trend
315 is associated with an overall decreased influence of Atlantic water corresponding well to
316 similar observations in the Nordic Seas (e.g. Hald et al., 2007; Skirbekk et al., 2010;
317 Slubowska et al., 2005). This also corresponds to north-western Europe lake and tree
318 records arguing for a late Holocene trend towards colder and dryer conditions (e.g.
319 Bjune et al., 2009; Kaufman et al., 2009). Nonetheless, at the Vøring plateau south of

320 the study site, planktic foraminiferal data show an overall increased influence of
321 Atlantic water throughout this time period (Andersson et al., 2003, 2010;
322 Risebrobakken et al., 2003). In addition to the overall cooling, the various proxy records
323 within the current study also argue for subtle changes within the oceanographic
324 conditions on a centennial temporal resolution throughout the late Holocene. These
325 fluctuations of the sub-surface water masses will be further discussed for four separate
326 time periods. Nonetheless, the strict ages of the boundaries as well as the following
327 interpretation should be taken with some caution due to the internal variability within
328 the different periods. But, in order to place the record within a geographically broader
329 context, it is compared with existing palaeo records and discussed in terms of possible
330 linkages to NAO conditions. The here interpreted fluctuating influence of sub-surface
331 water masses and their potential link with NAO conditions is presented as schematic
332 profiles across the northern Norwegian margin (Figure 7) [insert Figure 7].
333
334 *Period I: ca. 3500 – 2900 cal yr BP*

335 Between ca. 3500 and 2900 cal yr BP, the relative planktic foraminiferal abundances
336 show increased values of *G. uvula* (ca. 5 to 20 %) and high values (ca. 28 to 36 %) of *T.*
337 *quinqueloba* (Figure 3g and 3d). The latter has been associated with sub-polar
338 conditions and Atlantic water (Bé and Tolderlund, 1971; Volkmann, 2000), however it
339 has also considered to respond rapidly to changes in nutrient supply (Johannessen et al.,

1994; Reynolds and Thunnel, 1985). *G. uvula* has been associated with reduced salinities and Coastal water (Husum and Hald, 2012) as well as with high food supplies and cold productive surface waters (e.g. Bergami et al., 2009; Boltovskoy et al., 1996; Saito et al., 1981). Hence, the high relative abundances of both species strongly argue for an increased influence of colder and less saline Coastal water accompanied with a strong influence of a productive oceanographic front between Coastal and Atlantic water. In addition, both the increasing TOC and $\delta^{13}C$ values further argue for increased primary production corresponding to an increased influence of an oceanographic front (Figure 4c and 5b).

Contrary, the relatively low planktic foraminiferal concentrations and fluxes, as well as the in general low TOC values, seem to indicate a rather low primary production (Figure 4e and 4c). However, these values most likely result from the relatively poor preservation conditions as indicated by the generally high planktic foraminiferal fragmentation and the low $CaCO_3$ values (<22 wt. %) (Figure 4a and 4d). Nonetheless, the mean shell weight results actually show the highest values of the record, but this represents in all likelihood an artefact of the poor preservation conditions. Due to increased calcite dissolution, smaller species break more likely into fragments and thereby, attribute to a skewed sampling in this period with fewer available specimens. And thus, despite the use of a narrow size range, the remaining larger specimens might have led to the highest observed values of the record. Furthermore, as the solubility of

360 $CaCO_3$ increases with decreasing temperatures (Edmond and Gieskes, 1970), the here
361 recorded low $CaCO_3$ values argue for an increased influence of colder Coastal water
362 associated with enhanced dissolution conditions. Additionally, these low $CaCO_3$ values
363 might reflect the dilution by terrigenous material and thereby, support the interpretation
364 of enhanced carbonate dissolution at the continental margin off Norway (Huber et al.,
365 2000). However, the latter interpretation should be taken with caution as our age model
366 does not allow a detailed investigation of the sedimentation rate variability.

367 The depleting $\delta^{18}O_c$ trend can indicate an increased temperature and/or a
368 decreased salinity signal (Figure 5b). Furthermore, the planktic foraminiferal fauna data
369 and decreasing $SST_{Transfer}$ values from 7.2 to 6.8 °C (Figure 3h and 6c) strongly argue
370 for less saline water masses associated with an increased influence of Coastal water,
371 here most likely, reflected by the $\delta^{18}O_c$ record. Correspondingly, the reconstructed SSS
372 record confirms the overall trend towards less saline conditions (Figure 6d).
373 Nonetheless, contrary to decreasing $SST_{Transfer}$ values, the overall lower $SST_{Mg/Ca}$ values
374 remain somehow stable throughout this period (Figure 6c and 6b). The latter might
375 illustrate the different water depths and/or season that the two proxies represent possibly
376 arguing for more stratified water masses (Berben, 2014).

377 Overall, the multi-proxy data argue for an increased influence of relative cold
378 and fresh Coastal water and possibly more stratified water masses at the core site. This
379 might be related to a dominating negative NAO-like mode throughout this time interval

380 causing a more westwards located thinning wedge of Coastal water above Atlantic
381 water at the study site (Figure 7a). A 5200 year NAO-index has been reconstructed
382 using a multi-proxy geochemical record from a lake in south-west Greenland (Olsen et
383 al., 2012). Although this NAO-index generally shows mainly positive values, a stronger
384 influence of negative NAO conditions has been identified between ca. 4500 and 2500
385 cal yr BP which possibly correspond to the here suggested negative NAO-like
386 conditions (Figure 6e). In addition to this, the reconstruction of past atmospheric
387 circulation variability, based on exotic pollen analysis of marine sediments from
388 Newfoundland, illustrated a major shift from dominantly zonal (linked to a positive
389 NAO) to a more meridional (associated with a negative NAO regime) atmospheric
390 circulation pattern at ca. 3000 cal yr BP (Jessen et al., 2011). The latter are generally
391 associated with a reduced inflow of Atlantic water and a stronger influence of Coastal
392 water (e.g. Hurrell et al., 2013; Sætre, 2007). Correspondingly, between ca. 3500 and
393 2500 cal yr BP, the reconstructed SST record from the Vøring plateau (66.58° N, 07.38°
394 E) shows decreasing values arguing for a reduced influence of Atlantic water
395 (Andersson et al., 2003, 2010; Risebrobakken et al., 2003). Further, negative NAO
396 conditions resulted in a colder and dryer climate in north-western Europe (e.g. Wanner
397 et al., 2001). A decreasing temperature and precipitation trend throughout this time
398 interval was observed by pollen and plant macrofossil analyses from a lake record in
399 northern Norway (66.25° N, 14.03° E) (Bjune and Birks, 2008). Based on the mean

400 ablation-season temperature and winter snow accumulation, a decreased winter
401 precipitation was also observed between 3500 and 3200 cal yr BP in western Norway
402 (Nesje et al., 2001). Furthermore, surface ground temperatures were reconstructed by
403 applying the speleothem delta function to a measured $\delta^{18}O$ speleothem record from
404 northern Norway which also showed decreased values throughout this time interval
405 (Lauritzen and Lundberg, 1999).
406
407 *Period II: ca. 2900 – 1600 cal yr BP*

408 After ca. 2900 cal yr BP, a change in the planktic foraminifera's faunal distribution has
409 been recorded. Between ca. 2900 and 1600 cal yr BP, the latter is characterized by high
410 relative abundances of *N. incompta*, *T. quinqueloba*, *G. glutinata* and *G. bulloides*
411 (Figure 3c, 3d, 3e and 3f). These species have all been associated with subpolar
412 conditions and warm Atlantic surface water masses (e.g. Bé and Tolderlund, 1971;
413 Carstens et al., 1997; Johannessen et al., 1994; Simstich et al., 2003) and thus, argue for
414 a pronounced influence of Atlantic water brought to the study area by the NwAC.
415 Overall the total planktic foraminiferal concentration and flux values show
416 higher and increasing values, especially between ca. 2300 and 1600 cal yr BP, possibly
417 indicative of increased primary production (Figure 3a and 4e). However, at ca. 2900 cal
418 yr BP, the $\delta^{13}C$ record shows a clear shift towards depleted values at ca. 2300 cal yr BP
419 (Figure 5a). Thereafter, the $\delta^{13}C$ values remain relatively stable (ca. 0.3 ‰) and thus,

argue for less primary production throughout this period. The seemingly increased primary production as reflected by higher flux and concentration likely results from the generally improved preservation conditions. The slightly reduced fragmentation and increasing $CaCO_3$ values (up to ca. 30 wt. %) argue for a gradual trend towards reduced dissolution conditions throughout this period (Figure 4a and 4d). More favourable preservation conditions have previously been associated with increased influence of Atlantic surface water where pore waters are supersaturated with respect to calcium due to the lower organic matter productivity and a higher rain of $CaCO_3$ (e.g. Henrich et al., 2002; Huber et al., 2000).

The $\delta^{18}O_c$ record continues its depleting trend from period I possibly reflecting an increased temperature and/or reduced salinity signal (Figure 5b). The planktic foraminiferal fauna data and the clearly elevated $SST_{Transfer}$ values (ca. 7.4 °C) after ca. 2900 cal yr BP argue for increasing temperatures which are most likely related to an increased influence of Atlantic water (Figure 3h and 6c). Correspondingly, the palaeo SSS record shows overall higher values up to ca. 34 ‰ and thus, correlating to an increased influence of more saline Atlantic water (Figure 6d). In addition, the $SST_{Mg/Ca}$ record starts an increasing trend at ca. 2900 cal yr BP followed by higher values (ca. 0.5 - 1.0 °C higher than during period I) and thus, could also be linked to an increased influence of Atlantic water (Figure 6b).

439 The here recorded increased influence of Atlantic water might be caused due to
440 positive NAO conditions which are associated with stronger westerlies across the North
441 Atlantic (e.g. Hurrell et al., 2013). A close correlation between the NAO and the
442 longitudinal (east-west) extents of Atlantic water in the NwAC has previously been
443 observed (Blindheim et al., 2000). Positive NAO conditions result in a narrowing of the
444 NwAC and thereby, an enhanced influence of Atlantic water pushed closer towards the
445 Norwegian margin. This possibly reduced the influence of Coastal water at the study
446 area leading to a more eastwards located thinning wedge of Coastal water above
447 Atlantic water (Figure 7b). Throughout this time period, Olsen et al. (2012) observed a
448 general increasing trend in their NAO-index which might correspond to the here
449 interpreted influence of a positive NAO mode (Figure 6e). Similarly high sub-surface
450 temperatures associated with a strengthened inflow of Atlantic water have also been
451 observed at the Vøring plateau between ca. 2500 and 1600 cal yr BP (Andersson et al.,
452 2003, 2010; Risebrobakken et al., 2003). Additionally, increased temperatures in
453 northern Norway have been observed throughout this time interval from a lake record
454 (Bjune and Birks, 2008) and a speleothem record (Lauritzen and Lundberg, 1999).
455 Furthermore, between ca. 2700 and 1900 cal yr BP, increased winter precipitation has
456 been observed in western Norway (Nesje et al., 2001). These observations correlate well
457 to the warmer and wetter climate scenarios attributed to positive NAO conditions in
458 north-western Europe (e.g. Wanner et al., 2001).

Although the following interpretation might require a better age constrain on some of the here recorded main events, the last part of period II could be corresponding to the RWP observed between ca. 2000 and 1550 cal yr BP (ca. BCE 50 – CE 400) (Lamb, 1977). A period of warmer temperatures in northern Norway has also been linked to the RWP by Lauritzen and Lundberg (1999). Contrary to the relative warm RWP conditions in north-western Europe (e.g. Lamb, 1977), benthic foraminiferal and diatom data showed increased seasonal sea ice formation and reduced influence of Atlantic water between 2700 and 1600 cal yr BP in the Labrador Sea, south-west Greenland (Seidenkrantz et al., 2007). A general decreased influence of Atlantic water was also indicated by Irminger Current strength proxies on the southeast Greenland shelf between ca. 3600 and 1500 cal yr BP (Andresen et al., 2012). During a positive NAO mode, the subpolar gyre circulation is stronger and more east-west oriented, resulting in a reduced influence of the Irminger Current south of Greenland (Hatun et al., 2005; Sarafanov, 2009). Further, this opposite signal of a reduced Atlantic water component in the eastern part of the North Atlantic Ocean was suggested to result of a so called Atlantic oceanographic see-saw pattern in the climatic response to NAO changes (Seidenkrantz et al., 2007). This see-saw pattern of anomalously high ocean temperatures in the eastern versus anomalously low in the western parts of the North Atlantic Ocean during a positive NAO corresponds to a previous study on modern conditions by Wanner et al. (2001).

Period III: ca. 1600 – 900 cal yr BP

At ca. 1600 cal yr BP, the highest recorded values of both the planktic foraminiferal concentration and flux were followed by a sharp transition to low values (Figure 3a and 4e). The latter remained stable until ca. 900 cal yr BP. Further during this time interval, the planktic foraminiferal fauna shows more stable values for all species with particularly high values of *G. uvula* (ca. 15 to 27 %) (Figure 3g) which tolerates somewhat lowered salinities (e.g. Husum and Hald, 2012). These results likely reflect a stable period with a strong influence of Coastal water. Simultaneously, at ca. 1600 cal yr BP, the $CaCO_3$ record shifts towards an overall decreasing trend and the mean shell weight shows somewhat reduced values compared to period II (Figure 4d and 4b). This could indicate slightly reduced preservation conditions, possibly related to an enhanced influence of Coastal water and dilution of terrigenous material (e.g. Huber et al., 2000). Correspondingly, the $\delta^{13}C$ record increases after ca. 1600 cal yr BP which indicates enhanced primary production conditions and thereby, argues for a returned influence of Coastal water causing productive conditions near a stronger oceanic front (Figure 5a).

Although $\delta^{18}O_c$ values initially continue their decreasing trend towards ca. 1300 cal yr BP, they eventually increase and thereby, argue for a possible reduction in temperature (Figure 5b). All reconstructed water mass properties show at ca. 1600 cal yr BP a transition towards stable and lower values (Figure 6b, 6c, and 6d). Both the

499 $SST_{Transfer}$ (ca. 6.6 °C) and $SST_{Mg/Ca}$ records show lower values, down to 1.0 °C less
500 than the previous period II, hence indicating a reduced influence of relatively warm
501 Atlantic water (Figure 6c and 6b). The SSS record, in particular, shows a well
502 pronounced rapid decrease at ca. 1600 cal yr BP, and compared to period II, ca. 0.5 - 1.0
503 ‰ lower values. Hence, it also argues for a reduced influence of Atlantic water or an
504 enhanced influence of Coastal water (Figure 6d).

505 The multi-proxy data arguing for a shift towards a strong influence of Coastal
506 water is further interpreted as a westwards migrated thinning wedge of Coastal water
507 which might be associated with a change towards negative NAO conditions (e.g. Sætre,
508 2007) (Figure 7c). Within this time interval, the current multi-proxy record corresponds
509 well with other marine and terrestrial palaeorecords from the region. SST records from
510 the Vøring plateau have shown a sharp decrease at ca. 1600 cal yr BP, whereas the
511 values remained relatively low and stable compared to the previous period (Andersson
512 et al., 2003, 2010; Risebrobakken et al., 2003). This also suggests a reduced influence
513 of Atlantic water towards the core site. Further, a colder and dryer climate associated
514 with the DA was suggested by low surface ground temperatures between ca. 1500 and
515 900 cal yr BP in northern Norway (e.g. Lauritzen and Lundberg, 1999). Furthermore,
516 Bjune and Birks (2008) also observed decreasing air temperatures between ca. 1800 and
517 800 cal yr BP in northern Norway.

518 The here carefully suggested negative NAO conditions and its associated colder
519 and dryer climate in north-western Europe does however not correlate with the overall
520 positive NAO mode reconstructed by Olsen et al. (2012) during this time interval
521 (Figure 6e). Nonetheless, similar to period II, Seidenkrantz et al. (2007) observed an
522 opposite pattern of Atlantic water inflow contradictive with the deteriorate climate in
523 north-western Europe. In particular, their benthic foraminiferal record has been
524 indicating an increased influx of saline water brought to the Labrador Sea by the WGC
525 between 1600 and 1200 cal yr BP. These contradictory observations are attributed to the
526 previously mentioned Atlantic oceanographic see-saw pattern whereby an opposite
527 signal of ocean temperatures between the eastern and western North Atlantic Ocean has
528 been attributed to the dominating NAO mode (Wanner et al., 2001). Such a link
529 between SST anomalies in the subpolar gyre to a negative NAO and cold winters in
530 north-west Europe has also been made in previous studies (Luterbacher et al., 2002;
531 Miettinen et al., 2011). Based on fossil diatom assemblages from the northern subpolar
532 North Atlantic, a close link between NAO fluctuations and the strength variability of the
533 eastern and western branches of the NwAC has been indicated (Miettinen et al., 2011,
534 2012). During a negative NAO mode, weakened westerly winds over the Atlantic
535 results in profoundly increased influence of warm Atlantic water flowing westwards by
536 the IC (Miettinen et al., 2011, 2012). This close coupling between ocean and

atmosphere support the here interpreted negative NAO conditions throughout this period (Figure 7c).

Period IV: ca. 900 – 550 cal yr BP

The clearly decreasing values in the relative abundance of *G. uvula* after ca. 900 cal yr BP indicate a decreased influence of Coastal water (Figure 3g). The concomitant increase of *N. incompta* correspondingly suggest a stronger influence of subpolar conditions and thus, a stronger influence of Atlantic water (e.g. Bé and Tolderlund, 1971) (Figure 3c). Nonetheless, the increased abundance of *N. pachyderma* argues for increased polar conditions (e.g. Bé and Tolderlund, 1971; Volkmann, 2000) (Figure 3b) which is reflected by the reduced $SST_{Transfer}$ record reaching the lowest value (6.3 °C) of this study around ca. 550 cal yr BP (Figure 3h and 6c). Previously, proxy data from a Greenland ice core, used to reconstruct changes in atmospheric circulation patterns, indicated a shift at ca. 550 cal yr BP (ca. AD 1400) towards low sea level pressure associated with decreased SST in the North Atlantic (Meeker and Mayewski, 2002), which correlates well to the here observed reduced $SST_{Transfer}$ values. Further, a gently increased abundance of *N. pachyderma* was also found throughout the last ca. 1000 cal yr BP at the Vøring plateau (Risebrobakken et al., 2003). However, regardless of this similarity, the SST reconstructions from the Vøring plateau show increasing values during this time interval (Andersson et al., 2003, 2010; Risebrobakken et al., 2003). The

557 contradictory results of these records are most likely due to the use of different transfer
558 functions. The transfer function based on the >100 μm modern analogue data set used in
559 this study has previously indicated to result in generally lower temperatures (Husum
560 and Hald, 2012). Further, the potential influence of selective dissolution (e.g. Berger,
561 1970; Thunell and Honjo, 1981; Le and Thunell, 1996) might have altered the
562 foraminiferal assemblage composition resulting in an enrichment of the most
563 dissolution resistant thick-shelled species *N. pachyderma* (e.g. Metzler et al., 1982;
564 Hemleben et al., 1989). Additionally, the $SST_{Transfer}$ record in this study has been
565 reconstructed for a water depth of 100 m, whereas the SST record of the Vøring plateau
566 reflects temperatures at a 10 m water depth. These different represented water depths
567 however seem to mainly explain the overall lower SST values in this study, rather than
568 explaining the differences in trends (Husum and Hald, 2012). Wind induced mixing of
569 the surface layer is most likely responsible for the warmer temperatures at 10 m water
570 depth. Finally, the generally colder $SST_{Transfer}$ values are most likely due to the overall
571 cooling trend observed throughout the record and linked to decreasing solar insolation
572 values throughout the late Holocene (e.g. Hald et al., 2007; Kaufman et al., 2009).
573 After ca. 900 cal yr BP, the planktic foraminiferal concentrations and fluxes
574 slightly decrease which might indicate reduced primary production (Figure 3a and 4e).
575 The TOC record stabilizes after ca. 900 cal yr BP around somewhat lower values
576 compared to the end of period III which might indicate a small reduction in primary

577 production. The latter likely reflects a small shift away from productive oceanic front
578 conditions. At ca. 900 cal yr BP, both the fragmentation and mean shell weight records
579 show a pronounced increase (Figure 4a and 4b). The increased fragmentation argues for
580 deteriorated preservation conditions in the sediment, whereas the increased shell weight
581 indicates reduced dissolution of calcite. These conflicting interpretations might be best
582 explained by the different representation of these dissolution proxies and/or the different
583 influences affecting the results. The shell weight reflects the by dissolution caused mass
584 loss in an adult stage of *N. pachyderma*, whereas the fragmentation represents
585 fragments of all species including those of juvenile forms of *N. pachyderma*. Further,
586 environmental conditions such as nutrient availability, temperature and/or salinity can
587 affect the final shell weight during growth (e.g. Barker and Elderfield, 2002). The
588 fragmentation results could be affected by mechanical destruction during sieving which
589 might create an increased amount of fragments. Nonetheless, the relatively high and
590 stable $CaCO_3$ values, recorded after ca. 900 cal yr BP, are indicative of reduced
591 dissolution conditions (Figure 4d). The latter is associated with conditions marked by an
592 increased influence of Atlantic water (Huber et al., 2000). The increasing $\delta^{13}C$ record
593 might further indicate a reduced stratification at the core site resulting from an increased
594 influence of Atlantic water (Figure 5a).

595 Despite the overall cooling trend, several of the here presented proxies do argue
596 for changing oceanographic conditions after ca. 900 cal yr BP. The, in this study,

interpreted returned influence of Atlantic water might be the result of generally positive NAO conditions (Figure 7d). The reconstructed NAO-index from south-west Greenland also indicate positive NAO conditions during this time interval which are associated with the MWP (Olsen et al., 2012) (Figure 6e). Furthermore, this also corresponds to the results of a NAO reconstruction based on tree rings and speleothems that indicate a dominating positive NAO mode associated with an intensified AMOC (Trouet et al., 2009). These conditions are expressed by a reduced influence of Coastal water and a stronger moisture and heat transport to Norway by the NwAC resulting in warmer and wetter climatic conditions (e.g. Hurrell et al., 2013; Wanner et al., 2001). This correlates well to terrestrial records from northern Norway which show slightly increasing air temperatures for this time interval (Bjune and Birks, 2008) and high surface ground temperatures between ca. 800 and 500 cal yr BP (Lauritzen and Lundberg, 1999). Hence, this time interval possibly reflects the warmer conditions associated with the MWP which correlates with observation at the Vøring plateau between ca. 1150 and 650 cal yr BP (ca. 800 – 1300 AD) (Nyland et al., 2006) and in northern Norway between ca. 800 and 500 cal yr BP (ca. 1150 – 1450 AD) (Lauritzen and Lundberg, 1999). Between 1200 and 800 cal yr BP, a returned seasonal sea ice cover presumably related to relatively cold climatic conditions (relatively similar to the RWP) have been observed in the Labrador Sea with Atlantic water only entering as a weak subsurface current (Seidenkrantz et al., 2007). These observations correlate well to the

aforementioned oceanographic see-saw pattern resulting from positive NAO conditions (Miettinnen et al., 2011, 2012; Wanner et al., 2001).

Conclusions

A marine core from the northern Norwegian margin was investigated to elucidate the natural variability of water mass properties throughout the late Holocene on a centennial temporal resolution. In this study, a multi-proxy approach of palaeo sub-surface temperature and salinity data illustrated the palaeoceanographic evolution of the late Holocene. The latter was discussed in terms of changing influences of Atlantic and Coastal water. Due to the internal variability within the four different periods the suggested linkages to fluctuating modes of the NAO should be taken with caution. Nonetheless, the multi-proxy data allows for a broad interpretation and is therefore placed into a geographically wider context.

Overall, the proxy results indicate a general cooling trend throughout the late Holocene from ca. 8 to 6 °C ($SST_{Transfer}$). In addition, subtle fluctuating conditions of Atlantic and Coastal water intensity are observed during this time interval. Period I (ca. 3500 – 2900 cal yr BP) is influenced by relatively cold (ca. 6.8 °C, $SST_{Transfer}$) and less saline Coastal water and a stronger vertical stratification of the water column. These conditions might be linked to dominating negative NAO-like conditions. Throughout period II (ca. 2900 – 1600 cal yr BP), the core site experiences a stronger influence of

warm Atlantic water (ca. 7.4 °C, $SST_{Transfer}$) with more favourable preservation conditions possibly related to positive NAO conditions. The last part of this period might correspond to the RWP in north-western Europe. Stable conditions and cold sub-surface temperatures (ca. 6.6 °C, $SST_{Transfer}$) are observed within period III (ca. 1600 – 900 cal yr BP) indicating a returned and stronger influence of Coastal water. The conditions during this period are in this study attributed to a negative NAO mode and potentially correspond with the colder and dryer DA. Period IV (ca. 900 – 550 cal yr BP) shows a returned and stronger influence of Atlantic water which could be associated with dominating positive NAO conditions and the MWP. Nonetheless, Atlantic water reaching the core site was less warm (ca. 6.3 °C, $SST_{Transfer}$) compared to period II due to the overall late Holocene cooling. In addition, when comparing the results with previously published records, they indicated an opposite climatic response to changing NAO modes between the eastern and western North Atlantic Ocean and thereby, a close coupling between ocean and atmosphere within the climate system.

Acknowledgements

This work was carried out within the framework of the Initial Training Network program "Changing Arctic and Subarctic Environments" (CASE, Grant Agreement No. 238111) funded by the European Commission within the 7th Framework Program People, the Research Council of Norway in addition to UiT - The Arctic University of

657 Norway and the Norwegian Polar Institute. Jan Sverre Laberg is acknowledged for
658 providing the marine sediment core and Jochen Knies for access to the TOC and $CaCO_3$
659 data. Additionally, thanks are also extended to Jan P. Holm for his help preparing the
660 maps and Trine Dahl, Julia Sen and Karina Monsen for assisting with laboratory work
661 at UiT - The Arctic University of Norway. All new data, presented within this paper,
662 can be found within the supporting information file.
663

664 **References**

665 Andersson C, Risebrobakken B, Jansen E et al. (2003) Late Holocene surface ocean
666 conditions of the Norwegian Sea (Voring Plateau). *Paleoceanography* 18:
667 PA1044, doi: 10.1029/2001PA000654.
668 Andersson C, Pausata FSR, Jansen E et al. (2010) Holocene trends in the foraminifer
669 record from the Norwegian Sea and the North Atlantic Ocean. *Clim. Past* 6: 179-
670 193.
671 Andresen CS, Hansen MJ, Seidenkrantz MS et al. (2012) Mid- to late-Holocene
672 oceanographic variability on the Southeast Greenland shelf. *The Holocene* 0(0):
673 1-12. doi:10.1177/0959683612460789.
674 Aspeli R (1994) Late Quaternary benthic foraminiferal stratigraphy on the western
675 Barents slope Sea. Unpublished thesis, University of Tromsø (in Norwegian).

676 Barker S and Elderfield H (2002) Foraminiferal calcification response to glacial
677 interglacial changes in atmospheric CO_2. *Science* 297: 883-836.
678 Barker S, Kiefer T and Elderfield H (2004) Temporal changes in North Atlantic
679 circulation constrained by planktonic foraminiferal shell weights.
680 *Paleoceanography* 19: PA3008.
681 Bé AWH and Tolderlund DS (1971) Distribution and ecology of living planktonic
682 foraminifera in surface waters of the Atlantic and Indian Oceans. In: Funnell BM
683 and Riedel WR (eds) *The Micropaleontology of the Oceans*. Cambridge
684 University Press, London, 105-149.
685 Beer CJ, Schiebel R and Wilson PA (2010) Testing planktic foraminiferal shell weight
686 as a surface water [CO_3^{2-}] proxy using plankton net samples. *Geology* 38: 103-
687 106.
688 Berben SMP (2014) A Holocene palaeoceanographic multi-proxy study on the
689 variability of Atlantic water inflow and sea ice distribution along the pathway of
690 Atlantic water. University of Tromsø (PhD thesis).
691 Berben SMP, Husum K, Cabedo-Sanz P et al. (2014) Holocene sub-centennial
692 evolution of Atlantic water inflow and sea ice distribution in the western Barents
693 Sea. *Clim. Past* 10: 181-198, doi:10.5194/cp-10-181-2014.

694 Bergami C, Capotondi L, Langone L et al. (2009) Distribution of living planktonic
695 foraminifera in the Ross Sea and the Pacific sector of the Southern Ocean
696 (Antarctica). *Mar. Micropaleontol.* 73: 37-48.
697 Berger WH (1970) Planktonic foraminifera: Selective solution and the Lysocline. *Mar.*
698 *Geol.* 8 111-138.
699 Bjune AE and Birks HJB (2008) Holocene vegetation dynamics and inferred climate
700 changes at Svanåvatnet, Mo i Rana, northern Norway. *Boreas* 37: 146-156.
701 Bjune AE, Seppä H and Birks HJB (2009) Quantitative summer temperature
702 reconstructions for the last 2000 years based on pollen-stratigraphical data from
703 northern Fennoscandia. *J. Paleolimnol.* 41: 43-56.
704 Blindheim J, Borovkov V, Hansen B et al. (2000) Upper layer cooling and freshening in
705 the Norwegian Sea in relation to atmospheric forcing. *Deep-Sea Res. Pt. I* 47:
706 655-680.
707 Boltovskoy E, Boltovskoy D, Correa N et al. (1996) Planktic foraminifera from the
708 southwestern Atlantic (30°–60°S): Species-specific patterns in the upper 50 m.
709 *Mar. Micropaleontol.* 28: 53–72.
710 Broecker WS and Clark E (2001) An evaluation of Lohmann's foraminifera weight
711 dissolution index. *Paleoceanography* 16: 531-534.
712 Bryson RA and Goodman BM (1980) Volcanic activity and climate change. *Science*
713 207: 1041-1044.

714 Carstens J, Hebbeln D and Wefer G (1997) Distribution of planktic foraminifera at the
715 ice margin in the Arctic (Fram Strait). *Mar. Micropaleontol.* 29: 257-269.
716 Cifelli R (1961) Globigerina incompta, a new species of pelagic foraminifera from the
717 North Atlantic. Contributions Cushman Foundation Foraminiferal Research 12:
718 83-86.
719 Conan SMH, Ivanova EM and Brummer GJA (2002) Quantifying carbonate dissolution
720 and calibration of foraminiferal dissolution indices in the Somali Basin. *Mar.*
721 *Geol.* 182: 325-349.
722 Darling KF, Kucera M, Kroon D et al. (2006) A resolution for the coiling direction
723 paradox in Neogloboquadrina pachyderma. *Paleoceanography* 21: PA2011,
724 doi:10-1029/2005PA001189.
725 Duplessy JC, Ivanova E, Murdmaa I et al. (2001) Holocene paleoceanography of the
726 northern Barents Sea and variations of the northward heat transport by the
727 Atlantic Ocean. *Boreas* 30: 2-16.
728 Edmond JM and Gieskes TM (1970) On the calculation of the degree of saturation of
729 sea water with respect to calcium carbonate under in situ conditions. *Geochim.*
730 *Cosmochim. Acta* 35: 1261-1291.
731 Ehrmann WU and Thiede J (1985) History of Mesozoic and Cenozoic sediment fluxes
732 to the North Atlantic Ocean. Contributions to Sedimentology E.

733 Schweizerbart'sche Verlagsbuchhandlung, Stuttgart, 15: 1-109, ISBN 3-510-
734 57015-4.
735 Elderfield H and Ganssen G (2000) Past temperature and d18O of surface ocean waters
736 inferred from foraminiferal Mg/Ca ratios. *Nature* 405: 442-445,
737 doi:10.1038/35013033.
738 Elderfield H, Greaves M, Barker S et al. (2010) A record of bottom water temperature
739 and seawater [delta]18O for the Southern Ocean over the past 440 kyr based on
740 Mg/Ca of benthic foraminiferal Uvigerina spp. *Quaternary Sci. Rev.* 29: 160-
741 169.
742 Espitalié J, Laporte JL, Madec M et al. (1977) Méthode rapide de characterisation des
743 roches-mere, de leur potential petrolier et de leur degre d'évolution. *Revue de*
744 *l'Institute Francais du Petrole* 32: 23-42.
745 Giraudeau J, Jennings AE and Andrews JT (2004) Timing and mechanisms of surface
746 and intermediate water circulation changes in the Nordic seas over the last
747 10,000 cal years: A view from the north Iceland shelf. *Quaternary Sci. Rev.* 23:
748 2127-2139.
749 Hald M, Andersson C, Ebbesen H et al. (2007) Variations in temperature and extent of
750 Atlantic water in the northern North Atlantic during the Holocene. *Quaternary*
751 *Sci. Rev.* 26: 3423-3440.

752 Hatun A, Sand B, Drange H et al. (2005) Influence of the Atlantic Subpolar Gyre on the
753 Thermohaline Circulation. *Science* 309: 1841–1844.
754 Hemleben C, Spindler M and Anderson OR (1989) Modern Planktonic Foraminifera.
755 Springer-Verlag, New York, 363.
756 Henrich R, Baumann KH, Huber R et al. (2002) Carbonate preservation records of the
757 past 3 Myr in the Norwegian-Greenland Sea and the northern North Atlantic:
758 Implications for the history of NADW production. *Mar. Geol.* 184: 17-39.
759 Hopkins TS (1991) The GIN Sea: A synthesis of its physical oceanography and
760 literature review, 1972–1985. *Earth Sci. Rev.* 30: 175-318.
761 Huber R, Meggers H, Baumann KH et al. (2000) Recent and Pleistocene carbonate
762 dissolution in sediments of the Norwegian-Greenland Sea. *Mar. Geol.* 165: 123-
763 136.
764 Hurdle BJ (1986) The Nordic Seas. Springer, New York.
765 Hurrell JW, Kushnir Y, Ottersen G et al. (2013) An overview of the North Atlantic
766 Oscillation. In: Hurrell JW, Kushnir Y, Ottersen G et al. (eds) *The North Atlantic*
767 *Oscillation: Climatic significance and environmental impact.* American
768 Geophysical Union, pp. 1-35.
769 Husum K and Hald M (2012) Arctic planktic foraminiferal assemblages: Implications
770 for subsurface temperature reconstructions. *Mar. Micropaleontol.* 96(97): 38-47.

771 Ikeda M, Johannessen JA, Lygre K et al. (1989) A process study of mesoscale meanders
772 and eddies in the Norwegian Coastal Current. *J. Phys. Oceanogr.* 19: 20-35.
773 Jessen CA, Solignac S, Nørgaard-Pedersen N et al. (2011) Exotic pollen as an indicator
774 of variable atmospheric circulation over the Labrador Sea region during the mid
775 to late Holocene. *J. Quat. Sci.* 26(3): 286-296.
776 Jernas P, Klitgaard Kristensen D, Husum K et al. (2013) Palaeoenvironmental changes
777 of the last two millennia on the western and northern Svalbard shelf. *Boreas* 42:
778 236-255.
779 Jiang H, Eiriksson J, Schulz M et al. (2005) Evidence for solar forcing of sea-surface
780 temperature on the North Icelandic Shelf during the Late Holocene. *Geology*
781 33(1): 73-76.
782 Johannessen T, Jansen E, Flatøy A et al. (1994) The relationship between surface water
783 masses, oceanographic fronts and plaeoclimatic proxies in surface sediments of
784 the Greenland, Iceland, Norwegian Seas. In: Zahn R, Pedersen TF, Kaminski
785 MA and Labeyrie L (eds) *Carbon Cycling in the Glacial Ocean: Constraints of*
786 *the Ocean's Role in Global Change*. Berlin, Springer, 61-86.
787 Katz ME, Cramer BS, Franzese A et al. (2010) Traditional and emerging geochemical
788 proxies in foraminifera. *J. Foramin. Res.* 40(2): 165-192.
789 Kaufman DS, Schneider DP, McKay NP et al. (2009) Recent warming reverses long-
790 term Arctic cooling. *Science* 325: 1236-1239.

791 Knudsen KL (1998) Foraminiferer i Kvartær stratigrafi: Laboratorie og
792 fremstillingsteknik samt udvalgte eksempler. *Geologisk Tidsskrift* 3: 1-25.
793 Kozdon R, Eisenhauer A, Weinelt M et al. (2009) Reassessing Mg/Ca temperature
794 calibrations of Neogloboquadrina pachyderma (sinistral) using paired d44/40Ca
795 and Mg/Ca measurements. *Geochem. Geophys. Geosyst.* 10: Q03005,
796 doi:10.1029/2008GC002169.
797 Laberg JS, Vorren TO, Mienert J et al. (2002) The Trænadjupet slide: a large slope
798 failure affecting the continental margin of Norway 4,000 years ago. *Geo. Mar.*
799 *Lett.* 22: 19-24.
800 Lamb HH (1977) Climate, Present, Past and Future. Volume 2. Climatic History and the
801 Future. Methuen & Co Ltd, London, 835.
802 Lauritzen SE and Lundberg J (1999) Calibration of the speleothem delta function: an
803 absolute temperature record for the Holocene in northern Norway. *The Holocene*
804 9(6): 650-669.
805 Le JN and Thunnell RC (1996) Modelling planktic foraminiferal assemblages changes
806 and application to sea surface temperature estimation in the western equatorial
807 Pacific Ocean. *Mar. Micropaleontol.* 28:211-229.
808 Lean J (2002) Solar forcing of climate change in recent millennia. In: Wefer G, Berger
809 WH, Behre KE and Jansen E (eds) *Climate development and history of the North*
810 *Atlantic realm*. Berlin, Springer-Verlag, 75-88.

811 Lubinski DJ, Polyak L and Forman SL (2001) Freshwater and Atlantic water inflows to
812 the deep northern Barents and Kara seas since ca 13 ^{14}Cka: foraminifera and
813 stable isotopes. *Quaternary Sci. Rev.* 20: 1851-1879.
814 Luterbacher J, Xoplaki E, Dietrich D et al. (2002) Extending North Atlantic Oscillation
815 reconstructions back to 1500. *Atmos. Sci. Lett.* 2: 114-124,
816 doi:10.1006/asle.2001.0044.
817 Mangerud J, Bondevik S, Gulliksen S et al. (2006) Marine ^{14}C reservoir ages for 19th
818 century whales and molluscs from the North Atlantic. *Quaternary Sci. Rev.* 25:
819 3228-3245.
820 Mashiotta TA, Lea DW and Spero HJ (1999) Glacial interglacial changes in
821 Subantarctic sea surface temperature and d18O-water using foraminiferal Mg.
822 *Earth Planet. Sci. Lett.* 170: 417-432, doi:10.1016/S0012-821X(99)00116-8.
823 Meeker LD and Mayewski PA (2002) A 1400-year high-resolution record of
824 atmospheric circulation over the North Atlantic and Asia. *The Holocene* 12(3):
825 257-266.
826 Metzler CV, Wenkam CR and Berger WH (1982) Dissolution of foraminifera in the
827 Eastern Equatorial Pacific: an in situ experiment. *J. Foramin. Res.* 12(4): 362-
828 368.

829 Miettinen A, Koç N, Hall IR et al. (2011) North Atlantic sea surface temperatures and
830 their relation to the North Atlantic Oscillation during the last 230 years. *Clim.*
831 *Dyn.* 36: 533-543.
832 Miettinen A, Divine D, Koç N et al. (2012) Multicentennial variability of the sea
833 surface temperature gradient across the subpolar North Atlantic over the last 2.8
834 kyr. *J. Clim.* 25: 4205-4219.
835 Nesje A, Matthews JA, Dahl SO et al. (2001) Holocene glacier fluctuation of Flatebreen
836 and winter-precipitation changes in the Jostedalsbreen region, western Norway,
837 based on glaciolacustrine sediment records. *The Holocene* 11: 267–280.
838 Nyland B, Jansen E, Elderfield H et al. (2006) Neogloboquadrina pachyderma (dex. and
839 sin.) Mg/Ca and d18O records from the Norwegian Sea. *Geochem. Geophys.*
840 *Geosyst.* 7: Q10P17, doi:10.1029/2005GC001055.
841 Olsen J, Anderson NJ and Knudsen MF (2012) Variability of the North Atlantic
842 Oscillation over the past 5200 years. *Nature Geoscience* 5: 808-812. 28 July
843 2014, ftp://ftp.ncdc.noaa.gov/pub/data/paleo/paleolimnology/greenland/lake-
844 ss1220-2012.xls.
845 Orvik KA and Niiler P (2002) Major pathways of Atlantic water in the northern North
846 Atlantic and Nordic Seas toward Arctic. *Geophys. Res. Lett.* 29(19): 1896,
847 doi:10.1029/2002GL015002.

Ottersen G, Planque B, Belgrano A et al. (2001) Ecological effects of the North Atlantic Oscillation. *Oecologia* 128: 1-14.

Perkins H, Hopkins TS, Malmberg SA et al. (1998) Oceanographic conditions east of Iceland. *J. Geophys. Res.* 103: 21531-21542.

Pufhl HA and Shackleton NJ (2004) Two proximal, high-resolution records of foraminiferal fragmentation and their implications for changes in dissolution. *Deep-Sea Res. Pt. I* 51: 809-832.

Rasmussen TL and Thomsen E (2010) Holocene temperature and salinity variability of the Atlantic Water inflow to the Nordic Seas. *The Holocene* 20(8): 1223-1234.

Reimer PJ, Bard E, Bayliss A et al. (2013) Intcal13 and Marine13 radiocarbon age calibration curves. *Radiocarbon* 55(4): 1869-1887.

Reynolds L and Thunnel RC (1985) Seasonal succession of planktonic foraminifera in the subpolar North Pacific. *J. Foramin. Res.* 15: 282-301.

Risebrobakken B, Jansen E, Mjele E et al. (2003) A high resolution study of Holocene paleoclimatic and paleoceanographic changes in the Nordic Seas. *Paleoceanography* 18: 1017, doi:10.1029/2002PA000764.

Rørvik KL, Laberg JS, Hald M et al. (2010) Behavior of the northwestern part of the Fennoscandian ice sheet during the Last Glacial Maximum – a response to external forcing. *Quaternary Sci. Rev.* 29: 2224-2237.

867 Saito T, Thompson PR and Breger D (1981) Systematic index of recent and pleistocene
868 planktonic foraminifera. University of Tokyo press, Tokyo, 1-190.
869 Sarafanov A (2009) On the effect of the North Atlantic Oscillation on temperature and
870 salinity of the subpolar North Atlantic intermediate and deep waters. *ICES*
871 *Journal of Marine Science* 66(7): 1448-1454, doi:10.1093/icesjms/fsp094.
872 Seidenkrantz MS, Aagaard-Sørensen S, Sulsbrück H et al. (2007) Hydrography and
873 climate of the last 4400 years in a SW Greenland fjord: implications for
874 Labrador Sea palaeoceanography. *The Holocene* 17(3): 387-401,
875 doi:10.1177/0959683607075840.
876 Simstich J, Sarnthein M and Erlenkeuser H (2003) Paired δ18O signals of N.
877 pachyderma (s) and T. quinqueloba show thermal stratification structure in the
878 Nordic seas. *Mar. Micropaleontol.* 48: 107–125.
879 Skirbekk K, Klitgaard Kristensen D, Rasmussen TL et al. (2010) Holocene climate
880 variations at the entrance to a warm Arctic fjord: evidence from Kongsfjorden
881 trough, Svalbard. *Geological society, London, Special Publications*, 344: 289-
882 304, doi:10.1144/SP344.20.
883 Slubowska MA, Koç N, Rasmussen TL et al. (2005) Changes in the flow of Atlantic
884 water into the Arctic Ocean since the last deglaciation: Evidence from the
885 northern Svalbard continental margin, 80N. *Paleoceonography* 20: PA4014,
886 doi:10.1029/2005PA001141.

887 Slubowska-Woldengen M, Rasmussen TL, Koç N et al. (2007) Advection of Atlantic
888 Water to the western and northern Svalbard shelf since 17 500 cal yr BP.
889 *Quaternary Sci. Rev.* 26: 463-478.
890 Solignac S, Giraudeau J and De Vernal A (2006) Holocene sea surface conditions in the
891 western North Atlantic: Spatial and temporal heterogeneities. *Paleoceanography*
892 21: PA2004, doi:10.1029/2005PA001175.
893 Spielhagen RF and Erlenkeuser H (1994) Stable oxygen and carbon isotopes in planktic
894 foraminifera from the Arctic Ocean surface sediments: Reflection of the low
895 salinity surface water layer. *Mar. Geol.* 119: 227-250.
896 Stuiver M and Reimer PJ (1993) Extended 14C data base and revised CALIB 3.0 14C
897 age calibration program. *Radiocarbon* 35: 215-230.
898 Sætre R (2007) The Norwegian coastal current: Oceanography and Climate. Tapir
899 academic press, Trondheim, 89-99.
900 Thunell RC and Honjo S (1981) Calcite dissolution and the modification of planktonic
901 foraminiferal assemblages. *Mar. Micropaleontol.* 6:169-182.
902 Thornalley DJR, Elderfield H and McCave IN (2009) Holocene oscillations in
903 temperature and salinity of the surface subpolar North Atlantic. *Nature* 457:
904 711-714.

905 Trouet V, Esper J, Graham NE et al. (2009) Persistent positive North Atlantic
906 Oscillation mode dominated the Medieval Climate Anomaly. *Science* 324: 78-
907 80.
908 Vellinga M and Wood RA (2002) Global climatic impacts of a collapse of the Atlantic
909 thermohaline circulation. *Clim. Chang.* 54: 251-267.
910 Volkmann R (2000) Planktic foraminifers in the outer Laptev Sea and the Fram Strait:
911 Modern distribution and ecology. *J. Foramin. Res.* 30: 157-176.
912 Wanner H, Brönnimann S, Casty C et al. (2001) North Atlantic Oscillation – Concepts
913 and studies. *Surveys in Geophysics* 22: 321-381.
914 Wanner H, Beer J, Bütikofer J et al. (2008) Mid- to Late Holocene climate change: an
915 overview. *Quaternary Sci. Rev.* 27(19-20): 1-38,
916 doi:10.1016/j.quascirev.2008.06.013.
917 Werner K, Spielhagen RF, Bauch D et al. (2013) Atlantic Water advection versus sea-
918 ice advances in the eastern Fram Strait during the last 9 ka: Multiproxy evidence
919 for a two-phase Holocene. *Paleoceanography* 28: 283-295.
920 Zamelczyk K, Rasmussen TL, Husum K et al. (2013) Marine calcium carbonate
921 preservation vs. climate change over the last two millennia in the Fram Strait:
922 Implications for planktic foraminiferal paleostudies. *Mar. Micropaleontol.* 98:
923 14-27.

924 **Figure captions**

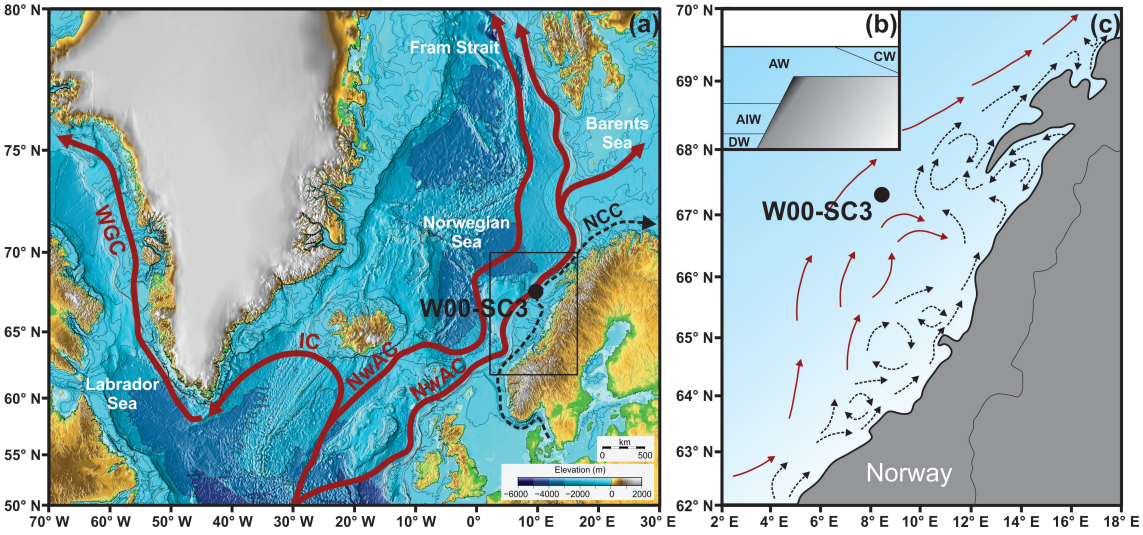

925

926 Figure 1. Study area of W00-SC3 (67.24° N, 08.31° E) (circle) with the main surface
927 currents: Norwegian Atlantic Current (NwAC), Irminger Current (IC), West Greenland
928 Current (WGC) and Norwegian Coastal Current (NCC). (a) Surface currents presented
929 on a bathymetric map. (b) Generalized schematic profile across the northern Norwegian
930 margin modified after Rørvik et al. (2010). Coastal water (CW), Atlantic water (AW),
931 Atlantic intermediate water (AIW) and Deep water (DW). (c) Detail map of the surface
932 currents nearby the core site modified after Sætre (2007). Full and dotted arrows
933 indicate Atlantic and Coastal water, respectively.

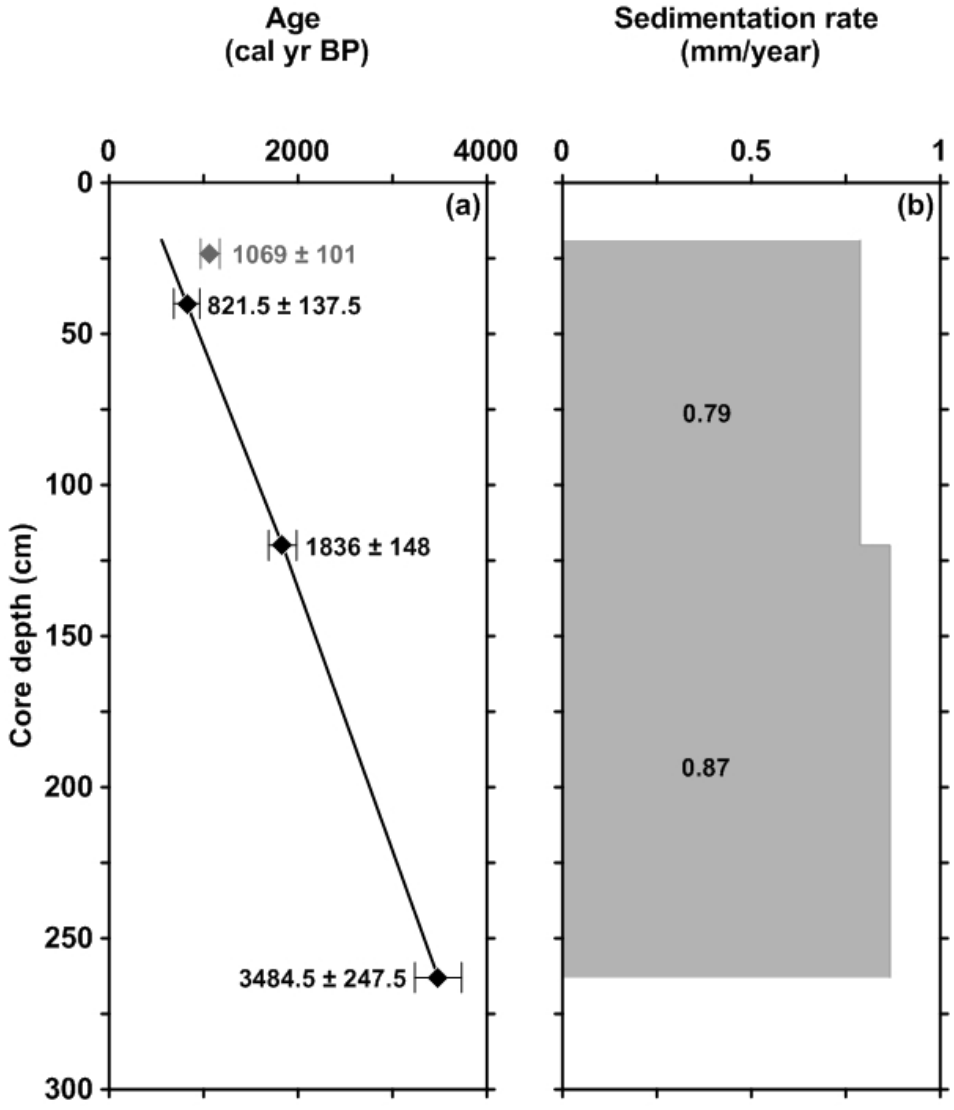

Figure 2. Depth-age model of W00-SC3 based on three calibrated AMS ^{14}C dates. The 2-σ range of the calibrated radiocarbon ages is indicated by an error bar. The exact values are noted in black for the used dates and grey for one omitted AMS ^{14}C date. (a) Calibrated calendar years BP versus core depth. (b) Sedimentation rates versus core depth.

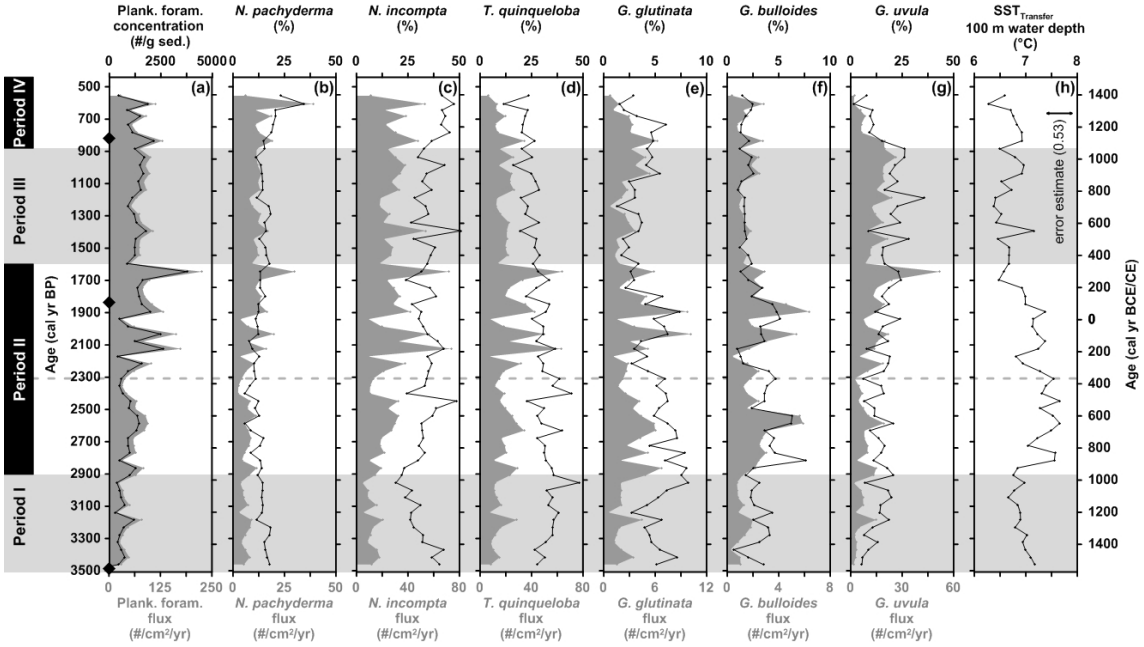

940

941 Figure 3. Planktic foraminiferal fauna versus cal yr BP (left y-axis) and cal yr BCE/CE
942 (right y-axis). The black diamonds on the Y-axis indicate the AMS ^{14}C converted to
943 calibrated radiocarbon ages. (a) Planktic foraminiferal concentration (black) and flux
944 (grey) versus age. (b-g) Species-specific relative abundances (black) and fluxes (grey)
945 of planktic foraminifera versus age. (h) Transfer function derived $SST_{Transfer}$ record
946 using a modern foraminiferal dataset by Husum and Hald (2012) versus age.

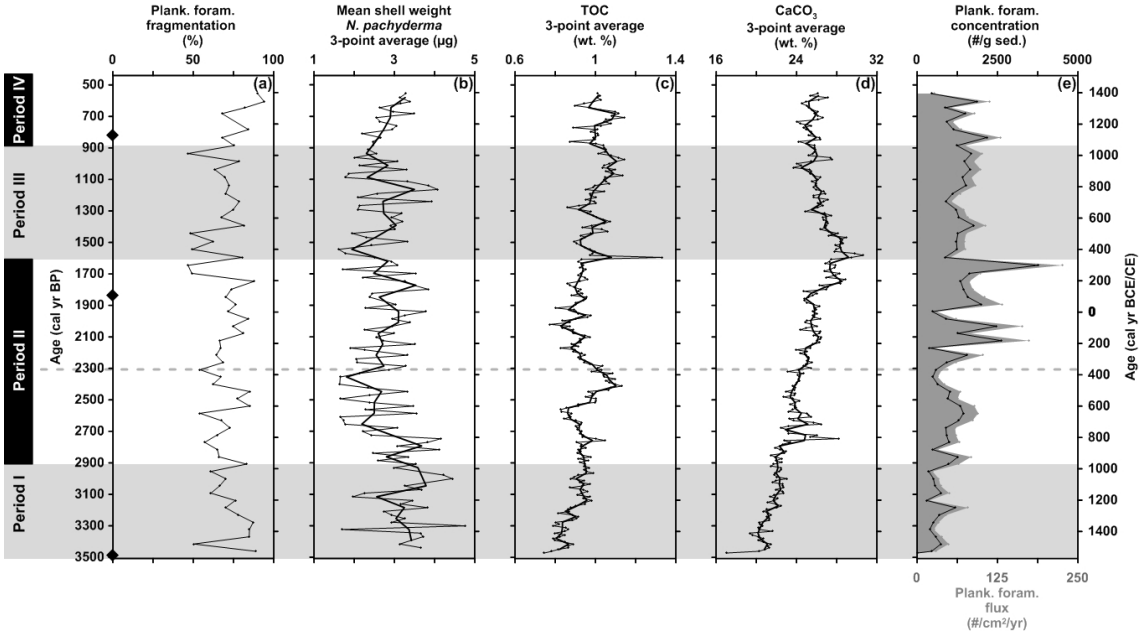

947

948 Figure 4. Preservation and geochemical analysis versus cal yr BP (left y-axis) and cal yr
949 BCE/CE (right y-axis). The black diamonds on the Y-axis indicate the AMS ^{14}C
950 converted to calibrated radiocarbon ages. (a) Planktic foraminiferal fragmentation
951 versus age. (b) Mean shell weight of *N. pachyderma* versus age. (c) Total organic
952 carbon versus age. (d) Calcium carbonate versus age. (e) Planktic foraminiferal
953 concentration (black) and flux (grey) versus age.

954

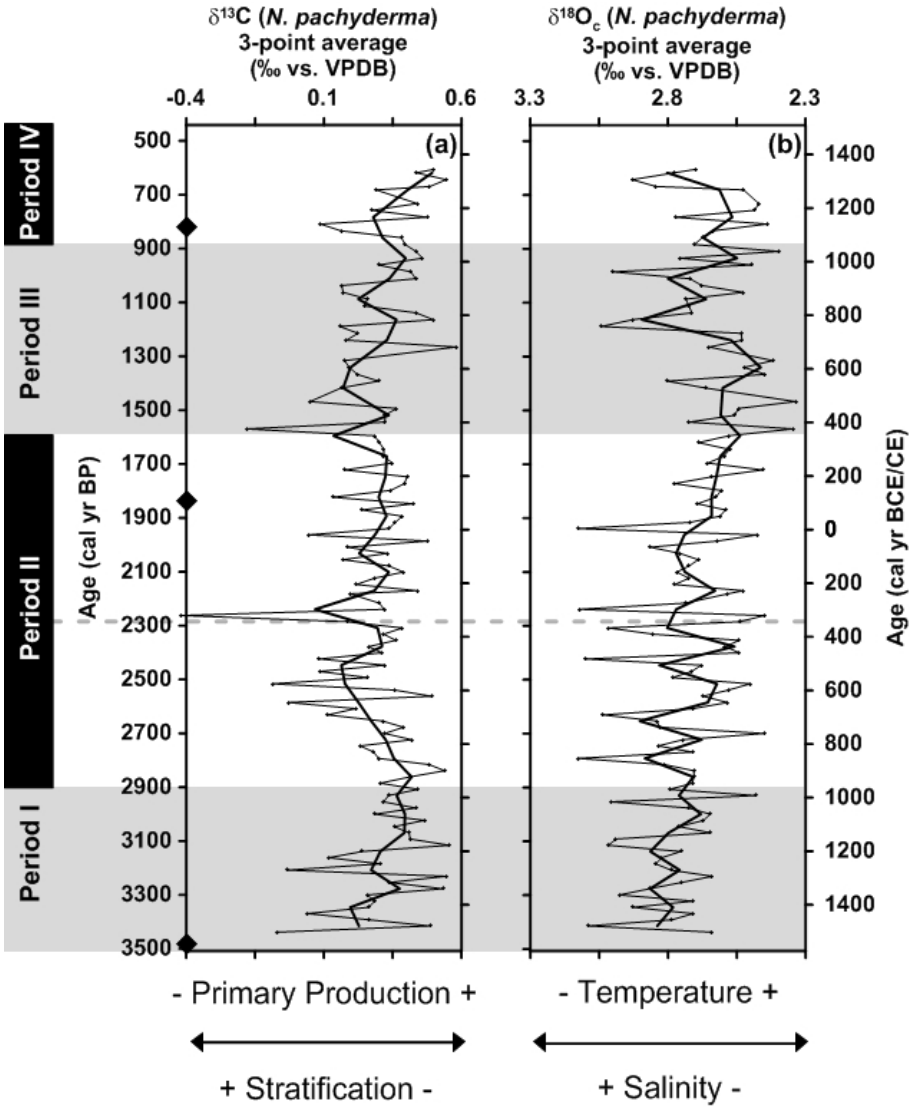

955

956 Figure 5. Stable isotopes analysis performed on *N. pachyderma* versus cal yr BP (left y-
957 axis) and cal yr BCE/CE (right y-axis). The black diamonds on the Y-axis indicate the
958 AMS ^{14}C converted to calibrated radiocarbon ages. (a) $\delta^{13}C$ measurements versus age.
959 (b) $\delta^{18}O_c$ measurements corrected for a vital effect of 0.6 ‰ according Simstich et al.
960 (2003) and Nyland et al. (2006) versus age.

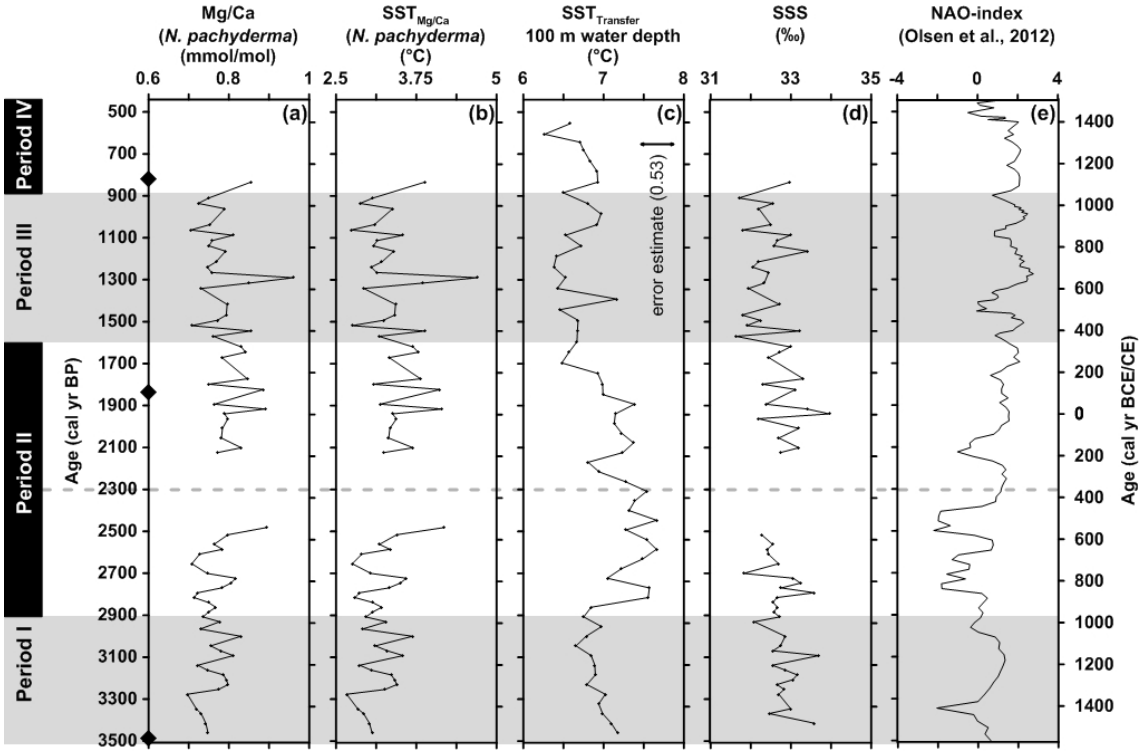

Figure 6. Reconstructed water mass properties versus cal yr BP (left y-axis) and cal yr BCE/CE (right y-axis). The black diamonds on the Y-axis indicate the AMS ^{14}C converted to calibrated radiocarbon ages. (a) Mg/Ca measurements of *N. pachyderma* versus age. (b) $SST_{Mg/Ca}$ record obtained by the temperature:Mg/Ca equation of Kozdon et al. (2009) versus age. (c) $SST_{Transfer}$ record using the modern foraminiferal dataset by Husum and Hald (2012) versus age. (d) SSS record derived by a combined foraminiferal (*N. pachyderma*) $\delta^{18}O_c$ and $SST_{Mg/Ca}$ approach using the salinity to $\delta^{18}O_w$ relation by Simstich et al. (2003) versus age. (e) Reconstructed NAO-index from a lake record in south-west Greenland (Olsen et al., 2012) versus age.

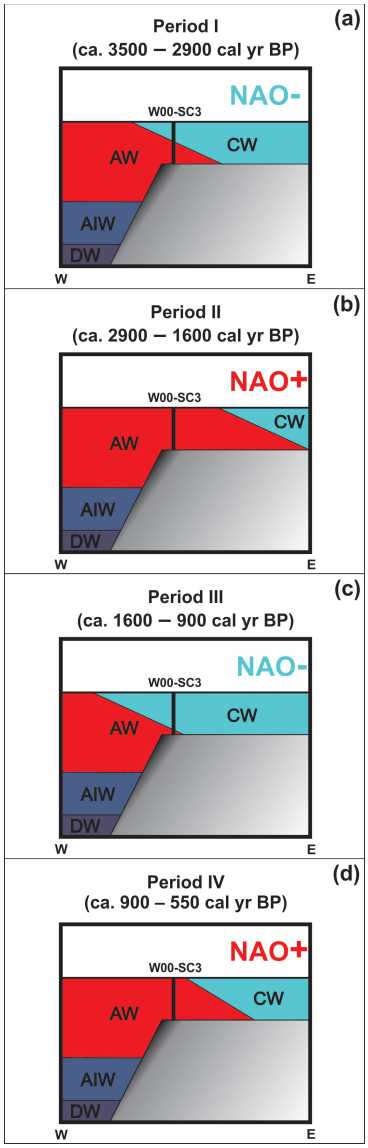

971

972 Figure 7. The interpretation of fluctuating influence of sub-surface water masses based
973 on multi-proxy data from the study area is presented as a schematic profile across the
974 northern Norwegian margin for four separate time periods. Coastal water (CW),
975 Atlantic water (AW), Atlantic intermediate water (AIW) and Deep water (DW).